




Facile fabrication of superhydrophobic nanocomposites coating materials using nanoemulsion polymerization technique and its application for protecting the petroleum carbon steel pipelines

M. R. Noor El-Din , A. I. Hashem,
R. E. Morsi, A. Abd El-Azeim, Reham H. Mohamed

Received: 10 March 2022 / Revised: 26 May 2022 / Accepted: 30 May 2022
© The Author(s) 2022

Abstract This paper aims to fabricate new superhydrophobic nanocomposite coating materials to protect the inner surfaces of the petroleum pipelines from corrosion. The batch emulsification polymerization technique (BEM) was used as a facial eco-friendly technique to prepare three hydrophobic (styrene/vinyl acetate) copolymers. The sol–gel method was used to prepare SiO₂ nanoparticles (SiO₂-NPs) with average size ranging from 90 to 101 nm. The functionalized SiO₂-NPs were prepared using hexadecyl trimethoxy silane (HDTS) as a precursor to increasing the hydrophobicity character of the unfunctionalized SiO₂-NPs. Three superhydrophobic [(styrene/vinyl acetate copolymer/functionalized SiO₂ nanoparticles (SiO₂NPs)] nanocomposites denoted as M1, M3, and M5 were fabricated by incorporating 1, 3, and 5 wt% of the functionalized-SiO₂NPs into the styrene/vinyl acetate copolymer, respectively. The effectiveness of the fabricated nanocomposite coating materials was analyzed using contact angle measurement and transmission electron and atomic force microscopies. The results showed that the highest contact angle of 161.21° was obtained by M5-nanocomposite. The highest

corrosion efficiency of 99.63% was obtained at 300 ppm concentration of M5-nanocomposite-coated solution, 298 K, and 24 days.

Keywords Superhydrophobic, Coating materials, Emulsion polymerization, Dipping method, Corrosion inhibition efficiency

Introduction

Corrosion is one of the most important problems facing the oilfield industries.¹ The most imperative factors affecting the increase in the corrosion rate of the petroleum pipelines are the high salinity of the formation water produced during crude oil production, hydrogen sulfide (H₂S), and carbon dioxide (CO₂) gases.² The oilfield industry is divided into three main sectors based on functions, processes, and operations. First, upstream oil and gas production sectors: The upstream activities include exploration, drilling, and extraction process. Natural gases and crude oil streams from production wells may be dry or wet depending on their water content and impurities. The presence of some impurities in the produced water such as salts and chlorides can enhance the corrosion rate and the formation of a localized type of attack.³ Besides the effect of the impurities in increasing the rate of corrosion, other factors such as temperature, pressure, flow rate, heat transfer, percentage of the associated water, and salt content in the produced crude oil increase the corrosion rate of carbon steel pipelines. The corrosion rate of upstream oil and gas pipelines is chemically reduced by using organic corrosion inhibitors or by coating the carbon steel pipes with highly water-resistant materials. Second, midstream sectors: The midstream activities include the storage tanks, treatment processing facilities, and transportation of the treated petroleum crude oil and natural gas. The

Supplementary Information The online version contains supplementary material available at <https://doi.org/10.1007/s11998-022-00669-z>.

M. R. Noor El-Din (✉)
R. E. Morsi, R. H. Mohamed
Egyptian Petroleum Research Institute (EPRI), 1Ahmed
El-Zomer St., Nasr City, Cairo 11727, Egypt
e-mail: mrned04@yahoo.com

A. I. Hashem
Faculty of Science, Ain Shams University, Abassia, Cairo,
Egypt

A. Abd El-Azeim
Khalda Petroleum Company, Cairo, Egypt

change in temperature and pressure at the oil gathering manifold and/or well-head causes a remarkable increase in the dissolved oxygen (DO) which, in turn, leads to an increase in the corrosion rate of the midstream facilities. Corrosion prevention is one of the most important considerations in protecting the production assets facility from corrosion.⁴ Third, the downstream sector: This sector specializes in refining and converting treated crude oil and gas into finished products. Recently, superhydrophobic (SH) nanocomposite materials were used to reduce the corrosion rate of the metal alloy to a minimum, thus improving the corrosion resistance of the coated metal surface.⁵ The SH materials were used to reduce the direct interaction between the corrosive media and the exposed surface of the carbon steel.⁶ The three main materials used for fabricating SH materials were inorganic (e.g., SiO₂ nanoparticles), organic such as polymers [e.g., polystyrene (PSt), poly(methyl methacrylate) (PMMA), etc.], and inorganic/organic hybrid materials (i.e., nanocomposites).⁷ There are many techniques used to fabricate the polymer matrix nanocomposites: in situ emulsion polymerization, sol–gel process, and melting extraction.⁸ The batch addition emulsification method is considered an eco-friendly method for the preparation of a highly stable nanoemulsion.⁹ Wang et al.¹⁰ reported SiO₂/polyacrylate nanocomposites enhanced the corrosion resistance of the mild steel specimens. Zuev¹¹ suggested that a strong reinforcement coating film used as an anticorrosion resistance film could be obtained by incorporating 0.5 wt% of fullerene nanofillers in an epoxy matrix. This work aims to fabricate three [(styrene/vinyl acetate copolymer)/functionalized SiO₂-NPs] nanocomposites denoted as M1, M3, and M5-nanocomposites as new superhydrophobic materials. These nanocomposites were prepared by incorporating 1, 3, and 5 wt% of the functionalized SiO₂-NPs into the C3-copolymer matrix, respectively. These materials are used to reduce the corrosion rate of the carbon steel pipelines in the oilfield industry to a minimum. The hydrophobicity character of the prepared coating materials was evaluated from the perspective of the static contact angle. The effect of the functionalized SiO₂-NPs concentration on the fabricated SH-coating materials' corrosion rate (mpy) was assessed by the weight loss technique (Rotating Cage Test). The surface topography of the coated films was analyzed using visual examination and scanning electron microscopy (SEM) after being exposed to synthetic brine water as corrosive media.

Materials and methods

Materials

Technical grades of styrene (St, > 99 wt%) and vinyl acetate (Vc, > 98 wt%) monomers were purchased from Sigma-Aldrich, Chemie GmbH-Schnellendorf, Ger-

many. Laboratory grades of Brij®30 and Pluronic® F-68 denoted as L and T, respectively, as nonionic emulsifiers were purchased from ACROS, Geel, Belgium. The analytical grade of STEPWET® DOS 70-DG denoted as R was purchased from Stepan, Northfield, IL, the USA. The technical grade of ammonium persulfate (>99 wt%) as initiator was purchased from Merck, Darmstadt, Germany. Analytical grade of hexadecyl trimethoxy silane as precursors was supplied by ACROS, Geel, Belgium. Technical grades of ammonia solution, trimethylamine, methanol, and benzene (Honeywell, Charlotte, NC, the USA) were used as received. Deionized water (DI) was used in all experimental procedures.

Petroleum produced water

Table S1 of the Supporting Information (SI) illustrates the physicochemical analysis of the produced water (formation water) of an oil-producing well (SQ-11 well), Karam field, Qarun Pet. Co., Western Desert, Egypt. The chemical composition of the synthetic brine water is illustrated in Table S2 (Table 2 is in the SI).

Methods

Preparation of emulsifier mixture

The batch addition method (BAM)⁹ was used to prepare a stable oil-in-water nanoemulsion. An emulsifier mixture denoted as RTL composed of three emulsifiers was used to form a stable (styrene/vinyl acetate) monomers/water nanoemulsion. The required hydrophilic-lipophilic balance (RHLB) used to form a stable (styrene/vinyl acetate) monomers-in-water emulsion was 14.¹² The optimal concentration of the used emulsifiers is calculated according to equation (1).¹³

$$\text{RHLB} = x_i \text{HLB}_R + 2x_i \text{HLB}_T + (1 - 3(x_i))\text{HLB}_L \quad (1)$$

where RHLB is the RHLB value of the oil phase used. The oil phase is composed of styrene and vinyl acetate. x_i , $2x_i$, and $(1 - 3x_i)$ are the mass fraction of emulsifiers R, T, and L, respectively. HLB_R , HLB_T , and HLB_L are the HLB values for emulsifier R (high HLB value), T (mediate HLB), and L (low HLB value).

Preparation of (styrene/vinyl acetate) copolymer (C3-copolymer)

Into a 500 mL semibatch reactor equipped with a condenser, a mechanical stirrer, and a thermocouple, 36.1 g of premixed monomers (styrene/vinyl acetate) with molar monomer ratios of (0.04:0.09), (0.06:0.08),

and (0.08:0.05), respectively, was separately added to 300 mL of the water phase with continuous stirring at a rotation speed of 600 rpm and temperature of 25°C. The water phase is composed of 4 g of RTL emulsifier mixture dissolved in 300 mL DI-water. After 15 min of obtaining a stable nanoemulsion of (styrene/vinyl acetate)/water, 0.065 wt% of ammonium persulfate was dropwise added to the previous stable emulsion. Afterward, the temperature of the reaction was raised to 65 ± 5°C, and the mixture was stirred at a rotation speed of 800 rpm. The precipitated copolymer was dried in a vacuum oven at 40°C until reaching a constant weight.¹⁴ The synthesis and separation procedures of the C3-copolymer were performed according to what was previously published procedure reported by reference (12).

Preparation of SiO₂ nanoparticles (SiO₂-NPs)

Uniform SiO₂ NPs were synthesized by the sol-gel processing technique.¹⁵ Into a 100 mL Erlenmeyer flask equipped with a magnetic stirrer and a thermostat, 1.6 mL of tetraethyl orthosilicate (TEOS) was dropwise added to a homogenous solution of ethanol (35.7 mL) and DI-water (5 mL) at a constant addition rate of 0.1 mL/5 min. The mixture was stirred at a constant rotation speed of 800 rpm and a constant temperature of 50 ± 5°C for 3 h. A mixture of ammonia (0.8 mL) and ethanol (0.9 mL) solution was added to the previous mixture to keep the pH value of the reaction within the range of 8–9. Thereafter, the mixture was agitated for a further 4 h at a constant temperature of 50 ± 5°C. After 24 h, a white powder of the SiO₂-NPs was precipitated. The precipitated SiO₂-NPs were filtered via a Whatman filter (Grade GF/F). The filtered SiO₂-NPs were centrifugated at a rotating speed of 20000 rpm. Afterward, the SiO₂-NPs were washed with ethanol 3–5 times and dried under a vacuum desiccator overnight at 25 ± 5°C temperature.¹⁵

Preparation of the functionalized SiO₂-NPs

The SiO₂-NPs prepared in the previous step were functionalized with hexadecyl trimethoxy silane (HDTS) to increase their hydrophobicity character.^{12,15} The typical process for preparing the functionalized SiO₂-NP is described in more detail in the Supporting Information (SI). The prepared functionalized SiO₂-NPs were denoted as an E-silicate.

Preparation of superhydrophobic nanocomposites

Three nanocomposites denoted as M1-, M3-, and M5-nanocomposites with distinct mechanical properties were prepared by incorporating 1, 3, and/or 5 wt% of E-silicate into the C3-copolymer matrix, respectively.¹²

The preparation of the superhydrophobic nanocomposites (M1, M3, and M5) is discussed in detail in the SI. Chemical characterizations of the prepared C3-copolymer, unfunctionalized SiO₂-NPs, and M1-, M3-, and M5-nanocomposites are described below.

The chemical characterization of the synthesized C3-copolymer, SiO₂-NPs, and the fabricated nanocomposites

FOURIER TRANSFORM INFRARED SPECTROSCOPIC (FTIR) ANALYSIS: The chemical structures of the synthesized C3-copolymer were justified using a Nicolet™ iN™10 Infrared Microscope, Thermo Fisher Scientific, Waltham, the USA. For this, 1.0 mg of C3-copolymer was ground and closely mixed with ~100 mg of dry potassium bromide (KBr) powder. Manual Hydraulic Press FTIR pellet press, SPECAC, the UK was used to form the KBr disks or pellets for FTIR analysis.

HIGH-RESOLUTION TRANSMISSION ELECTRON MICROSCOPY (HRTEM): The morphology and microstructure of the unfunctionalized SiO₂-NPs deposited on carbon steel coupons were characterized by high-resolution transmission electron microscopy (HRTEM, Model JEM-200CX, JEOL, Japan) at an accelerating voltage of 200 kV.

DYNAMIC LIGHT SCATTERING (DLS) MEASUREMENTS: The average droplet size distribution (Z_{avg}) and the polydispersity index (PDI) of the synthesized C1, C2, and C3-copolymers were analyzed by DLS (Zetasizer Nano ZS, Malvern Instruments, Worcestershire, UK) at a scattering angle of 173° with an argon-laser ($\lambda = 488$ nm). The measurements were performed in triplicate with three readings for each. The average droplet size (Z_{ave}) was calculated from the diffusion coefficient measurement using the Stokes-Einstein equation [equation (2)] as follows:

$$D = \frac{kT}{3\pi\eta Z_{avg}} \quad (2)$$

where D is the diffusion coefficient, k is the Boltzmann constant, T is the absolute temperature, and η is the viscosity of the medium. The droplet size and size distribution were determined using a **CONTIN** analysis mode.

ATOMIC FORCE MICROSCOPY (AFM): The surface topographies of carbon coupons coated by C3-copolymer M5-nanocomposites were evaluated by a NanoScope IV atomic force microscope using a controller equipped with a hybrid 153 scanner (Veeco/Digital Instruments (DI), Santa Barbara, CA) at six different points through the scanned surface.

CONTACT ANGLE (CA) MEASUREMENTS: Static contact angles of uncoated and carbon steel surfaces coated with C3-copolymer, functionalized SiO₂-NP, and (M1-, M3-, and M5-) nanocomposites were measured by Theta optical tensiometer, Attension-Biolin Scientific Company, Finland. Measurements were carried out by placing a water droplet of $\pm 0.5 \mu\text{L}$ on the surface of a carbon steel coupon using a manual precision syringe dispenser (C205M). USB 3.0 digital camera with LED-based background lighting, $62 \times 62 \text{ mm}$, was used to photograph water droplets settling on uncoated and coated carbon steel surfaces.

Evaluation of the coated carbon steel coupons as anticorrosion coating materials

The efficiency of the fabricated nanocomposites as new anticorrosion coating materials was evaluated by the weight loss technique. Uncoated and coated coupon surfaces were photographed using optical microscopy and scanning electron microscopy (SEM) as follows.

CORROSION INHIBITION EFFICIENCY MEASUREMENTS:

a. Dip-coating process

Dip-coating is a common coating technique¹⁶ used for fabricating a high protection layer on carbon steel surfaces. In the present work, the dip-coating method was used to fabricate a highly adhesive coating film of C3-copolymer and M5-nanocomposite, with a film thickness of 90–120 μm , on the surface of carbon steel coupons. Dip-coating consists of a four-step process: First, pretreatment-step: Four uncoated coupons with a standard dimension of $2.5 \times 6 \text{ in.}^2$ were sonicated in ethanol for 10 min to remove any hydrocarbon materials from the surface. Afterward, the coupons were sanded to create a rough coupon surface before being coated. The sanded coupons were rinsed with acetone, DI-water, and dried by hot air. Second, immersion-step: The sanded coupons were dipped into the 10 wt% coating solution at a constant speed. The coating solution was composed of 10 g of one C3-copolymer and/or M5-nanocomposite dissolved in 100 mL of toluene. The coupons remained in the coating solution for 20 min to form a homogenous film with a thickness of 60–90 μm . Third, withdrawal step: The precoated coupons were slowly withdrawn from the solution at a constant speed to avert the deformation of the built-up coated film. The thickness of the coated film depends on the speed with which the coupons are withdrawn and the viscosity of the coated solution. The slower the pull, the thinner the coating layer. Forth, etching (drying) step: The coated carbon steel coupons resulting from the previous step were placed in the DRIE chamber to create a low-energy surface film on the surface of the coated coupons. At this point, a protective coating layer of C3-copolymer and/or M5-nanocomposite was deposited over the

surface of the carbon steel coupon. The anticorrosion performance of the coated coupon surfaces was evaluated by the rotating cage test as discussed below. This test should be implemented at conditions that simulate the field operational conditions.

b. Rotating cage (weight loss) test

The rotating cage (RC) test¹⁷ is a standard laboratory simulation test used to evaluate the corrosion resistance of the carbon steel pipelines under field operating conditions. In this study, the RC test was used to estimate the corrosion rate of the carbon steel coupons coated with C3-copolymer and M5-nanocomposite in the presence of brine synthetic water as a corrosive media. According to the American Standard Test Method (ASTM G 184-06), eight coupons (one of the eight coupons was an uncoated coupon (blank) and the rest were coated coupons) of known weight were supported between two PTFE disks (0.8 cm diameter) mounted at 75 mm from the bottom of the stirring rod. Two 0.1 cm holes were drilled in the top and bottom of the PTFE plates. These holes are approximately 15 mm away from the center of the PTFE plates. These perforations increased the turbulence flow of the crude fluid over the surface of the coated coupons. In our test, the hydrocarbon fluid consists of a mixture of crude oil and produced water as a corrosive media. The ratio of crude oil to the produced water in the hydrocarbon fluid used reflects the actual ratio of crude oil to the produced water recorded in the daily production report of the well used (SQ-11 well). If a crude oil sample is not available from the SQ-11 well, diesel fuel or any suitable hydrocarbon fluid may be used. The RC-test measurement was performed at conditions close to field operating conditions. In a typical procedure, seven coated coupons and one uncoated coupon were immersed in a vessel containing 7.5 L of the hydrocarbon fluid. The effect of the concentration of the coated materials as 100, 200, and 300 ppm deposited on the coupon surface was evaluated at a rotating speed of 1000 rpm, 1 bar atmosphere, 298 K, and immersion time of 24 days. After 24 days, the tested coupons were withdrawn from the crude fluid solution, rinsed three times with acetone and then with distilled water, and dried under vacuum at a temperature of 25°C. The weight loss (W , mg) measurement is used to calculate the efficiency ($E\%$) of the coated materials as follows [equation (3)]¹⁸:

$$E\% = \frac{w_o - w_i}{w_o} \quad (3)$$

where W_o and W_i are the average weight losses of uncoated and coated coupons at different concentrations of the coated material deposited on the coupon surfaces, respectively.

The corrosion rate of the coated coupons is calculated according to the following [equation (4)]:

$$\text{Corrosion rate}(C_r), \text{ mpy} = \frac{(C \times W)}{C \times A \times T} \quad (4)$$

where C is a constant ($C = 143.7$), W is the weight loss (g), D is the density of the carbon steel coupon (g/cm^3), A is the surface area of the carbon steel coupon (cm^2), and T is the exposure time of the tested coupons to the corrosive media (h). The carbon steel alloy is No.1018, UNS code of G10180, with a density of $7.86 \text{ g}/\text{cm}^3$ and CORRATER Multiplier of 1.00.

SURFACE TOPOGRAPHY MEASUREMENTS: The surface topography of the uncoated and coated coupon surfaces after exposure to corrosive media was assessed by optical microscopy and scanning electron microscopy as follows.

a. Optical microscopy inspections

The surface topography of uncoated and carbon steel coupons coated with C3-copolymer and M5-nanocomposite was investigated by Olympus CX33 optical microscopy, model, Shinjuku Monolith, Tokyo, Japan.

b. Scanning electron microscopic (SEM) measurements

The surface topography of uncoated and carbon steel coupons coated with C3-copolymer and M3-nanocomposite after exposure to corrosive media was analyzed by scanning electron microscopy (SEM) technique. SEM is a precise technique used to detect the performance of the coating, localized corrosion pits count, and the surface topography of the coupon surfaces coated with C3-copolymer and M5-nanocomposite after and before exposure to corrosive media. SEM analysis was conducted by JEOL JSM-820 (JEOL, Tokyo, Japan) with a tungsten filament gun and Carl Zeiss Supra with a FEG. SEM has scanned the coated surface by magnification power of 300000 times. The investigated coated samples were deposited on suitable beveled microscopy holders and sprayed with a gold/palladium alloy under vacuum to improve the image resolution. The deposition of gold/platinum alloy on the coated surface was performed by a sputter coater.

Results and discussion

FTIR spectroscopy analysis of C3-copolymer

Figure S1 (Supporting Information) shows the FTIR spectrum of the prepared C3-copolymer. From Fig. S1, a characterization peak at $\nu = 2981 \text{ cm}^{-1}$ was assigned to the stretching vibration peak of the aliphatic C-H group. The absorption resonance at $\nu = 3095.76 \text{ cm}^{-1}$ is assigned to the C-H of aromatic stretching vibration bands of the phenyl ring. Absorption stretching bands that exist at 1607.14 , 1490.86 , and 1473.69 cm^{-1} are

assigned to C=C in-plane stretching vibration bands of the phenyl ring. The out-of-plane stretching band at $\nu = 759.34 \text{ cm}^{-1}$ indicates the C-C of an aromatic ring vibration. The presence of the previous peaks confirms the presence of the repeating units of styrene molecules. Furthermore, carbonyl acetate ester and ester C-O stretching bands appear at $\nu = 1738$ and 1236 cm^{-1} , respectively. The appearance of the previous new bands indicated the presence of vinyl acetate moiety beside the styrene moiety in the C3-copolymer.¹² As shown in Fig. S1, the stretching broadband at $\nu = 3409 \text{ cm}^{-1}$ was attributed to the presence of a trace amount of moisture (O-H group) in the sample. This moisture was due to the utilization of emulsifiers during the polymerization step that includes the O-H group in its structure. The use of the emulsifiers at a concentration higher than the critical micelle concentration (CMC) during the polymerization process resulted in the formation of fine micelles within the polymer matrix. These micelles were difficult to remove from the polymer network during the purification step.¹² Further elucidation techniques used to confirm the preparation of polystyrene (PSt), unfunctionalized SiO_2 -NPs, C3-copolymer, and M5-nanocomposite were briefly reported by Noor El-Din et al.¹²

Dynamic light scattering (DLS) measurements

The effect of (styrene: vinyl acetate) monomer ratios as (0.04:0.09), (0.06:0.08), and (0.08:0.05) for C1-, C2-, and C3-copolymers prepared, respectively, at a constant RLT concentration of 0.50 wt%, ammonium persulfate (initiator) concentration of 0.065 wt%, and emulsification temperature of $60 \pm 5^\circ\text{C}$ on the resulted copolymer droplet size is depicted in Figs. 1a–1c, respectively. From Figs. 1a–1c, the droplet size of the synthesized C1- and C3-copolymer increased from 106.7 to 109.8 nm with decreasing the styrene ratio in the synthesized C1- and C3-copolymer from 0.08 to 0.04, respectively. Reducing the proportion of styrene in the synthesized copolymers increased the diffusion rate of the initiator from the water phase to the micelle of the monomer formed. Increasing the initiator concentration enhanced the emulsion polymerization, thereby, decreasing the droplet size of the copolymer formed. Meaning, increasing the number of the nucleated micelles enhanced the emulsion polymerization process.¹⁹ The lower concentration of the styrene monomer and the shorter time of the nucleation step minimized the dispersed micelle to flocculate and form a smaller droplet size. As shown in Fig. 2, the C3-copolymer-coated sheet showed a good hydrophobicity character compared with C1- and C2-copolymers synthesized (the glass surface was used instead of the carbon steel coupon to show the water droplets slipping on the coated surface). Increasing the hydrophobicity character of the coated surface coated by C3-copolymer increased the sliding of a drop of water on the surface. Increasing the hydrophobicity character of surface

coated with C3-copolymer was due to the increased molar ratio of styrene moiety in the C3-copolymer. Increasing the percentage of styrene moiety promoted the formation of strong covalent bonds between the C3-copolymer matrix and the functionalized E-silicate, which increased the hydrophobicity properties of the coated film (discussed later).¹² Accordingly, the C3-copolymer is best suited for nanocomposite fabrication as indicated below.

Preparation of unfunctionalized $\text{Si}_2\text{O-NPs}$

Figure S2 shows slightly heterogeneous $\text{SiO}_2\text{-NPs}$ with particle sizes ranging from 90 to 101 nm. The slight accumulation of the $\text{SiO}_2\text{-NPs}$ resulted in the entanglement between the different sizes of the dispersed $\text{SiO}_2\text{-NPs}$. The obtained $\text{SiO}_2\text{-NPs}$ were spherical with a slightly heterogeneous particle size distribution. The heterogeneous shape improved the static segregation of the dispersed particles with little potential for accumulation.¹²

Fabrication of superhydrophobic nanocomposites

To enhance the hydrophobicity character of C3-copolymer, different concentrations of the E-silicate as 1, 3, and 5 wt% were incorporated into the C3-copolymer matrix to form three nanocomposites namely, M1-, M3-, and M5-nanocomposites, respectively. The surface topography and the wettability character of the water droplet placed on the coupons coated by the fabricated nanocomposites were analyzed by SEM, AFM, and contact angle analysis as described in the following sections.

Scanning Electron Microscopic (SEM) measurements

Figure 3 depicts the surface morphology of the coated coupons by M5-nanonanocomposite. From Fig. 3, the surface topography of the M5-nanocomposite network displays collapsible dens and a highly crimped surface with internal air cavities through the network. The functionalized E-silicate exhibited a homogeneous distribution with a little lumping of the dispersed particle through the M5-nanocomposite-coated surface. The integration of the functionalized E-silicate into the C3-copolymer matrix caused the coated coupon surface to be more wrinkled. Increasing the surface crimped increased the roughness of the coated surface, which led to a decrease in the surface wettability.²⁰

Atomic force microscopic (AFM) analysis

The surface topography of uncoated and carbon steel surface coated with C3-copolymer and M5-nanocomposite is depicted in Figs. 4a–4c. Figure 4a represents the AFM image of the uncoated carbon steel surface. Figures 4 b–4 c reflect the impact of coating materials of C3-copolymer and M5-nanocomposite on the surface roughness and topography of coated coupons. From Fig. 4b, the topography of the carbon steel surface coated with C3-polymer showed a uniform surface with little roughness and helical-like structures along the coated surface. This phenomenon may be due to the lack of E-silicate as filler adhesive material incorporated in the copolymer matrix.²¹ Decreasing the roughness degree of the coated surface promoted the corrosion rate of the pipeline's coating surface. On the other hand, the presence of E-silicate incorporated into the C3-copolymer matrix enhanced the surface hydrophobicity and the surface roughness of the coated film, which led to an increase in the water contact angle

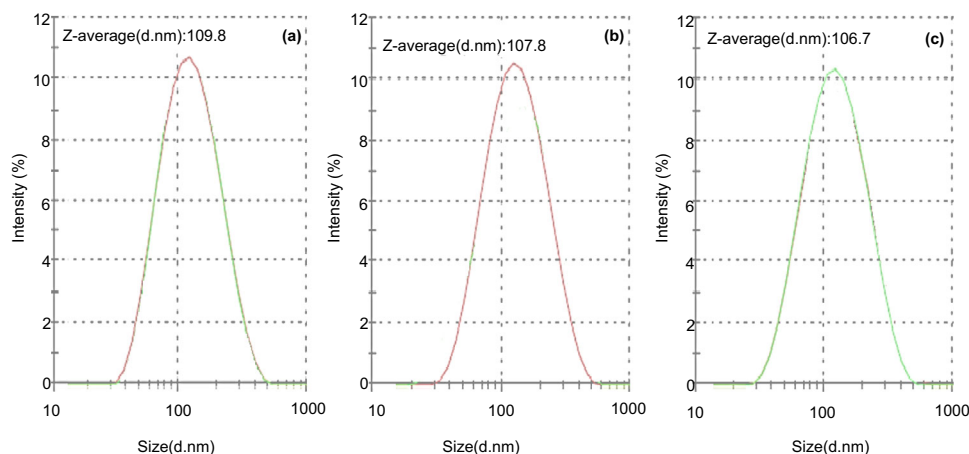


Fig. 1: (a–c): Effect of (styrene: vinyl acetate) monomer ratios of (a) 0.04:0.09, (b) 0.06:0.08, and (c) 0.08:0.05, respectively, on the resulted droplet size (nm) after emulsion polymerization at RLT concentration of 0.50 wt%

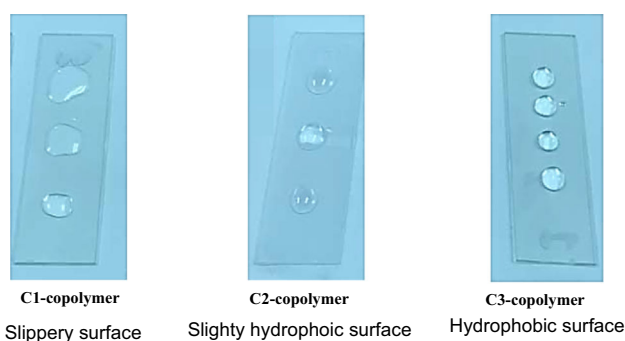


Fig. 2: The effect of the styrene molar ratio on the hydrophobic properties of the glass surface coated with C1, C2, and C3-copolymers

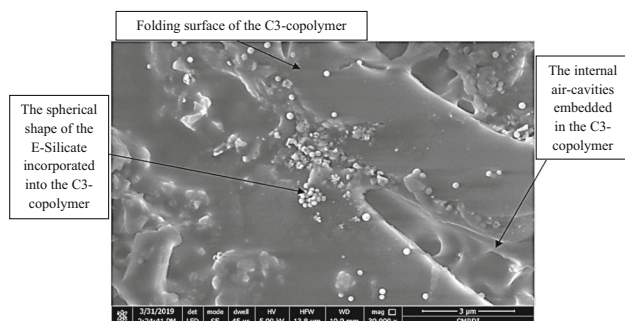


Fig. 3: SEM patterns of the synthesized M5-nanocomposite at 5 wt% of the E-silicate

to meet the optimum value ($CA < 150^\circ$). From Fig. 4c, a noticeable amendment in the surface topography with a hierarchical structure was observed. The reason for increasing the hierarchical structure of the coated film is evidently due to the presence of E-silicate in the C3-copolymer matrix. Increasing the E-silicate in the fabricated nanocomposite changed the mechanical (i.e., tensile strength, modulus of elasticity, etc.) and the physicochemical properties of M5-nanocomposite rendering it more convenient when used as a coating material. The alteration of the mechanical properties of the M5-nanocomposite resulted from the formation of strong covalent crosslinking between the hydrophobic part of the E-silicate and the C3-copolymer network. These crosslinking networks resulted in the formation of a superhydrophobic film with durable properties.¹²

Contact angle

Based on the contact angle (CA) measurement, carbon steel coupons are divided into two categories: first, hydrophilic surface ($40 < CA < 90^\circ$) and second, hydrophobic surface ($90 < CA < 110^\circ$).²² As shown in Table 1, the static contact angle (CA) increased from 71.95 to 100.32° by increasing the E-silicate concentration from 0 to 3 wt%, respectively. The increase in the CA value of the coupons coated by E-silicate was

attributable to an increase in the roughness characterization of the coated film. The presence of various water-repellent materials such as the folding network of C3-copolymer and unequal particle size of the functionalized E-silicate in M1-, M3-, and M5-nanocomposites caused the contact angle of the coated coupons to increase. The results in Table 1 revealed that the contact angle increased from 132.35 to 161.21° with increasing the E-silicate concentration from 1 to 5 wt% in M1- and M5-nanocomposites fabricated, respectively. As can be seen from the SEM pattern in Fig. 3, the folding structure of the C3-copolymer matrix and the asymmetric particle size of the functionalized E-silicate create entrapped air cavities on the coated surface. These cavities with different structures, shapes, and sizes reinforced the roughness structure of the coating film, which, in turn, led to an increase in the contact angle to be superhydrophobic ($CA = 161.21^\circ$).²³ However, increasing the concentration of embedded E-silicate increased the number of internal air cavities, increased the surface roughness of the coated surface, and, consequently, increased the contact angle.²⁴ From the previous results, the nanocomposite with the lowest droplet size and the highest contact angle ($CA = 161.21^\circ$) was M5-nanocomposite. Thus, the M5-nanocomposite will be evaluated as an anticorrosion coated material.

Assessment of the coated coupons as anticorrosion material

Based on ASTM G-184-06, the corrosion resistance of the carbon steel coupons coated with C3-copolymer and/or M5-nanocomposite solution was assessed using the weight loss technique. The effect of the coating solution concentration of C3-copolymer and M5-nanocomposite, exposure time of the coated coupons to the corrosive media, and the temperature on the inhibition efficiency of the coated coupons is described below.

Effect of the coating solution concentration

The effect of the coating solution concentration of C3-copolymer and/or M5-nanocomposite on the weight loss (mg) and Cr (mpy) for coupons coated at 298 K and exposure time of 24 days is depicted in Fig. 5 and illustrated in Table 2. The coating solution was composed of 2 g of a C3-copolymer and/or M5-nanocomposite dissolved in 100 mL of benzene. The results in Table 2 showed that the inhibition efficiency of the coated coupons with M5-nanocomposite decreased from 99.63 to 98.10% as the concentration of coating solution of M5-nanocomposite in the corrosive media increased from 100 to 300 ppm, respectively. This decrease in the inhibition efficiency may be attributed to increasing the concentration of M5-nanocomposite injected into the brine water. An

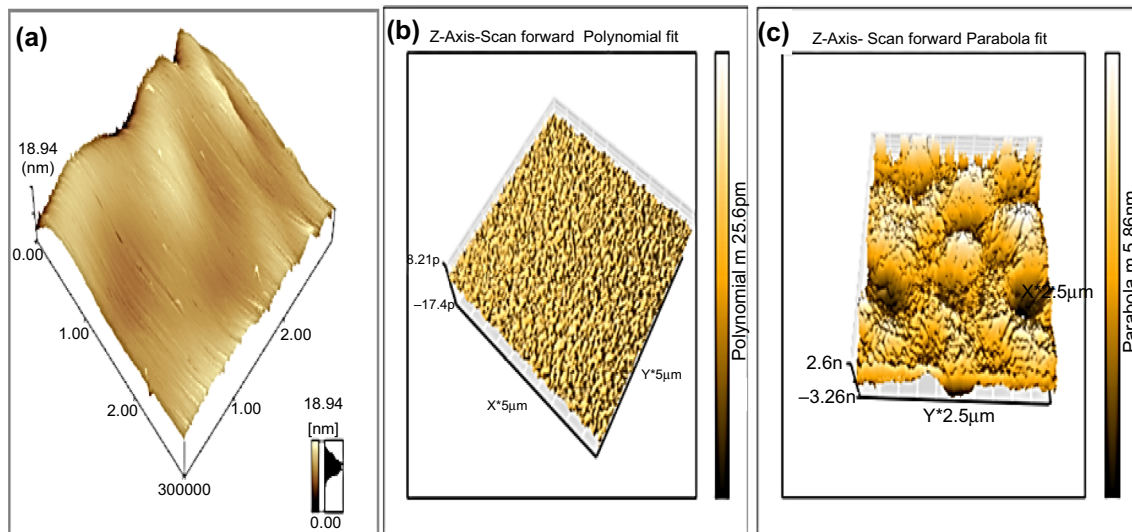


Fig. 4: (a–c): AFM topographies of (a) uncoated carbon steel and carbon steel coupons coated by (b) C3-polymer and (c) M5-nanocomposite

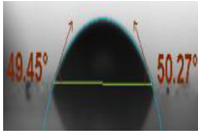
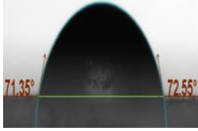
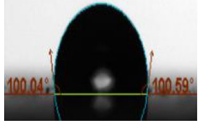
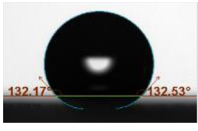
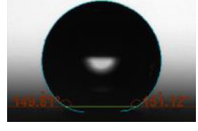
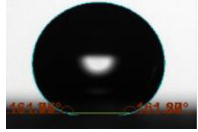
increase in the M5-nanocomposite concentration in the feeding dose from 100 to 300 ppm increases the roughness topography of the coated surface. Increasing the roughness of the coated surface was due to the fabrication of a strong adhesive-coated film with a helical-like structure on the coated coupon surfaces. This helical-like structure prevents direct contact between the coated surface and the corrosive media.²⁵ As shown in Fig. 5, at 100 ppm concentration of C3-copolymer and M5-nanocomposite, the curves are divided based on exposure time into two regimes: First, from 0 to 8 days, the rate of the weight loss (mg/cm^2) for the coated coupons is nearly constant. Second, from 8 to 24 days, the weight loss of the coated coupons for C3-copolymer and M5-nanocomposite increased significantly with increasing the exposure time from 8 to 24 days. This means that increasing the exposure time increased the degradation rate of the coated coupons. Increasing the time exposure of the exposed coupon surface to the corrosive medium increased the likelihood of the protective coated film to damage and increased the oxidation–reduction reaction upon the surface of coupons, therefore, increasing the corrosion rate.¹⁸ Table 2 represents the inhibition efficiency (η , %) and corrosion rate (mpy) of uncoated and coated carbon steel coupons with C3-copolymer and M5-nanocomposite at exposure time of 24 days and 298 K. From Table 2, the corrosion rate (mpy) decreased from 3.7 to 1.5 mpy for the coated coupons with C3-copolymer and M5-nanocomposite, respectively. The reason behind this behavior was attributed to the rough structure of the coated film, which resulted from the presence of E-silicated embedded in the M5-nanocomposite matrix. Decreasing the corrosion rate of the coated coupons with M5-nanocomposite was due to increasing the E-silicated in its network, which led to an increase in the physico-chemical interaction between the coupon surface and

the coated materials. Subsequently, the coated surface became more water-repellent (superhydrophobic).¹² These superhydrophobic layers boost the ability of the coated coupons to retard direct contact between the corrosive media and the surface of the coated coupons.

Effect of exposure time

The effect of exposure (immersion) time on the inhibition efficiency of uncoated and carbon steel coupons coated with C3-copolymer and M5-nanocomposite was assessed at 100 ppm, 298 K, and exposure time of 24 days, as illustrated in Fig. 5. The results in Fig. 5 reveal that the weight loss (mg/cm^2) of the M5-nanocomposite coated surface increased from 0 to 1.9×10^{-2} as the exposure time increased from 0 to 24 days, respectively. From Table 2, the corrosion rate (mdd) of the coupons coated with C3-copolymer and M5-nanocomposite decreased, respectively, from 48.6 to 24.9 mdd, respectively, at 100 ppm concentration, 298 K, and 24 days. The decrease in the corrosion rate is attributable to the efficiency of the silicated coating layer that coats the surface of the coupon to reduce the direct impact of corrosive media on the coupon surface. The 5 wt% of E-silicate embedded in the M5 nanocomposite enhanced the corrosion protection properties of the coated surface by forming nano/microoverlapped layers with hierarchical structures at different heights.²⁶ This hierarchical structure prevents the diffusion of the aggressive ions from the corrosive bulk solution to the metal surface of the coupon used.²⁷ Figure 6 demonstrates the schematic diagram of the adsorption and the prospective anticorrosive mechanism of M5-nanocomposite on the coupon substrate. The bilateral-plan adsorbed on the surface of the coupon coated with the M5-nanocomposite increased the roughness structure of the coating layer and the

Table 1: Contact angle (θ) measurements of uncoated and coated carbon steel with (C3-copolymer), (E-silicate), and (M1-, M2-, M3-composites) at different concentrations of E-silicate as (0), (3), and (1, 3, and 5) wt %, respectively

Composite	The concentration of the E-silicate incorporated into the C3-copolymer matrix, wt %	Contact angle (θ)
Uncoated carbon steel surface	0	49.86 \pm 0.41 
Carbon steel surface coated with C3-copolymer	0	71.95 \pm 0.6 
E-silicate ^a	3	100.32 \pm 0.28 
Composite ^b M1	1	132.35 \pm 0.18 
M3	3	150.50 \pm 0.6 
M5	5	161.21 \pm 0.1 

^aConcentration of E-silicate deposited on the carbon steel surface is 3 wt%.

^bConcentration of E-silicate incorporated into the C3-copolymer matrix is 1, 3, and 5 wt%.

internal air-caves structure of the coating layer; consequently, the corrosion inhibition efficiency of the coated surface to the corrosive media increased with respect to time.

Effect of temperature

Figure 7 represents the effect of temperature on the corrosion rate (Cr) of uncoated and the coated coupons with C3-copolymer and M5-nanocomposite at 298, 313, and 333 K and 24 days. The results in Fig. 7 show that the corrosion rate (Cr) of the M5-nanocomposite increased from 24.9 to 60.5 mdd with increasing the temperature from 298 to 333 K, respectively. From Table 3, at a constant concentration of a coating solution of 100 ppm and a temperature of 333 K, the

difference in the coating material used to coat the carbon coupons significantly affects the corrosion rate. As shown in Table 3, the Cr decreased from 84.3 to 60.5 mdd as the concentration of the E-silicate embedded in C3-copolymer and M5-nanocomposite increased from 0 to 5 wt%, respectively, at 100 ppm of the coating solution in brine water and 333 K. The reason for increasing the Cr when using C3-copolymer was due to the formation of a semismooth structure of the coated surface. On the other hand, the surface topography of the surface coated with M5-nanocomposite was rough with a nano-/microstructure profile. This structure enhanced the coated materials to form the air-pocket structure along the surface of the coupon material. These air pockets reduce the thermal effect of corrosive media on the thickness of the coating layers; thereby, it can isolate the surface of the coated

Table 2: Inhibition efficiency (η) and the corrosion rate of uncoated and coated coupons for C3-copolymer and M5-composite concentration of 100 ppm and (100, 200, and 300 ppm), respectively, 298 K, and 24 days

Coated carbon steel coupons	E-silicate concentration, wt%	The concentration of the coating solution ^a , ppm, that was injected into the brine water	The inhibition efficiency (η), %	Corrosion rate (C_r)	
				Milligram per dm ² per day (mdd)	Mille-inch per year (mpy)
Untreated coupon (blank)	0	0	0	163.1	11.6
C3-copolymer	0	100	86.07	48.6	3.7
		100	98.10	24.9	1.5
M5-composite	5	200	99.21	10.4	0.6
		300	99.63	4.9	0.3

^aCoating solution composed of 2 g of C3-copolymer and/or M5-composite dissolved in 100 mL benzene.

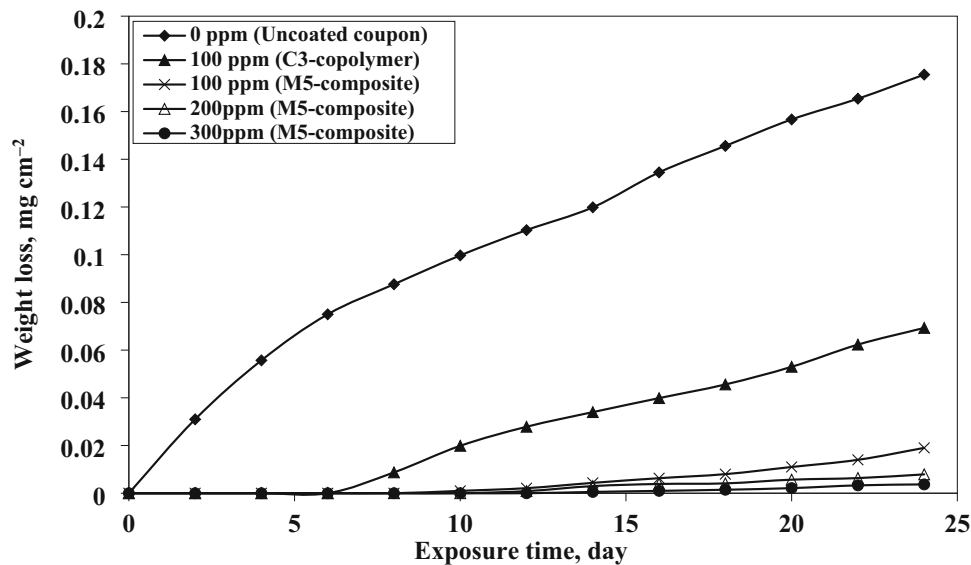


Fig. 5: Weight loss (g) versus time (day) for uncoated and coated carbon steel coupons with C3-copolymer and M5-composite at a coating solution concentration of (100 ppm) and (100, 200, and 300 ppm), respectively, and 298 K

layer from the thermal effect of corrosive media.²⁸ Thus, the effect of temperature on the efficiency of the coating layer is reduced to the lowest level.

Table 3 depicts the activation energy (E_a) values of C3-copolymer and M5-nanocomposite at 298, 323, and 333 K. The activation energy (E_a) is calculated using the Arrhenius equation [equation (5)]²⁹ as follows:

$$\ln(C_r) = \frac{-E_a}{R} \left(\frac{1}{T} \right) + \ln(b) \quad (5)$$

where C_r is the corrosion rate of the coated coupons, R is the Universal gas constant ($8.314 \text{ J mol}^{-1}\text{K}^{-1}$), T is the absolute temperature, and b is the preexponential factor which depends on the coupon alloy type. A plot of corrosion rate ($\ln(C_r)$) obtained by weight loss

measurement versus $1/T$ (K^{-1}) gave a straight line as depicted in Fig. 7. The slope of the line is equal to $-E_a/(2.303R)$. The results in Table 3 show that the value of the activation energy (E_a) reduced from 25.1 to $17.2 \times 10^{-4} \text{ kJ/mol}$ as the percentage of the E-silicate embedded in the coating material of C3-copolymer and M5-nanocomposite increases from 0 to 5 wt%, respectively. Increasing the E_a value was attributed to an increase in the adhesion force between the coating material and the carbon steel substrate, the high hydrophobicity character of the coating layer, and a highly effective physical barrier between the metal and corrosive media that prevents charge transfer of the corrosive ions from the bulk to the surface of the coupon, which in turn, reduces the corrosion rate of the carbon steel surfaces.²⁹ The respective activation energy of 25.1 kJ/mol is in good agreement with the

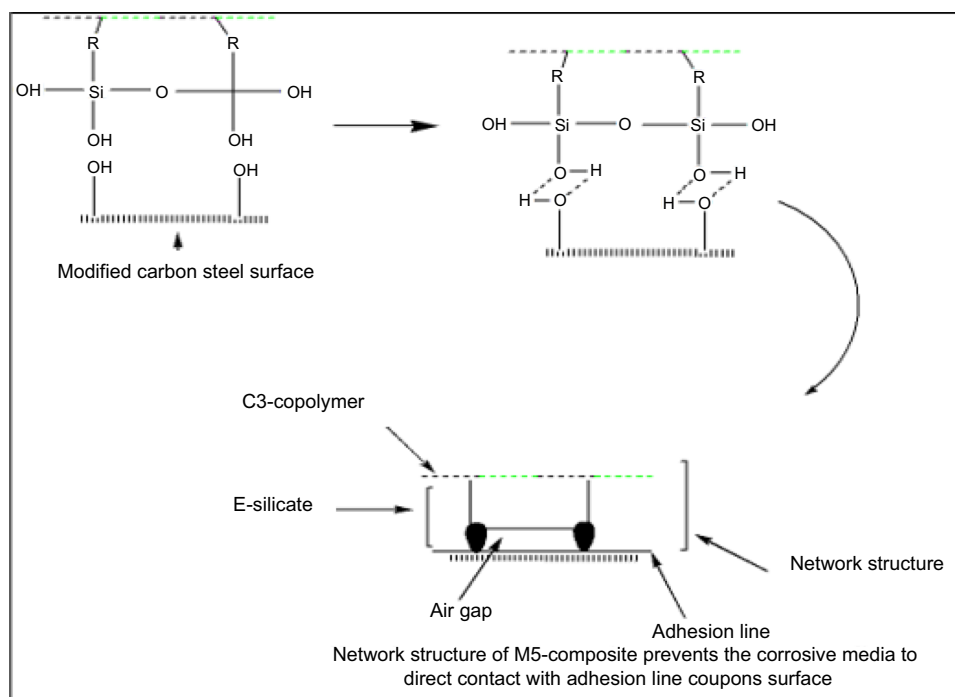


Fig. 6: Schematic diagram demonstrating the structural configuration of M5-composite on the carbon steel surface

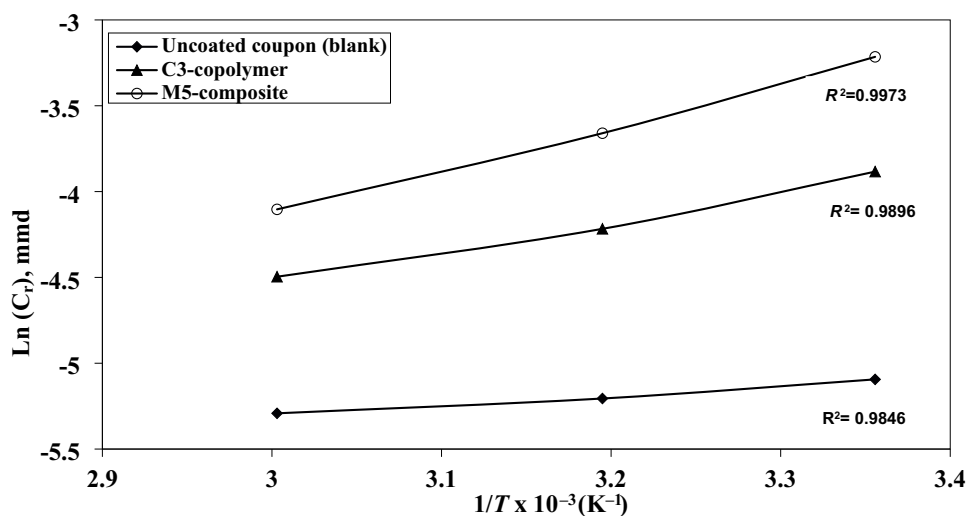


Fig. 7: A plot of $\ln(C_r)$ vs $1/T$ of uncoated and carbon steel coupons coated with C3-copolymer and M5-nanocomposite at a coating solution concentration of (0 ppm) and (100 and 100 ppm), respectively, and different temperatures of 298, 313, and 333 K

literature and support the physical adsorption of coated coupons ($E_a > 20$ kJ/mol).¹⁸

Effect of contact angle

The effect of C3-copolymer and M5-nanocomposite coating materials on the corrosion rate of the coated coupons (mpy) with respect to the resulting contact angles (θ) is demonstrated in Fig. 8. The results in

Fig. 8 revealed that the corrosion rate diminished from 3.7 to 1.5 mpy as the water contact angle (θ) of the C3-copolymer and M5-nanocomposite increased from 101.37 to 163.77°, respectively, after 24 days. The increase in the contact angle may be attributed to the E-silicate effect. With the increase in the proportion of E-silicate in the coated material, the hydrophobicity character of the coating coupons increases, and consequently, the contact angle of the M5-nanocomposite increased compared with that of the C3-copolymer.¹²

Table 3: Activation energy (E_a) of uncoated and coated carbon steel coupons with C3-copolymer and M5-composite at 0, 100, and 100 ppm, respectively, and different temperatures of 298, 313 and 333 K

Coated carbon steel coupons	Conc. of the coating solution, ppm, that was injected into the brine water	Temp., K	Corrosion rate (C_r), mdd	The activation energy (E_a), $\times 10^{-4}$ kJ/mol
Untreated coupon (blank)	0	298	163.1	5.5
		313	182.3	
		333	198.7	
C3-copolymer	100	298	48.6	17.2
		313	67.8	
		333	84.3	
M5-composite		298	24.9	25.1
		313	44.1	
		333	60.5	

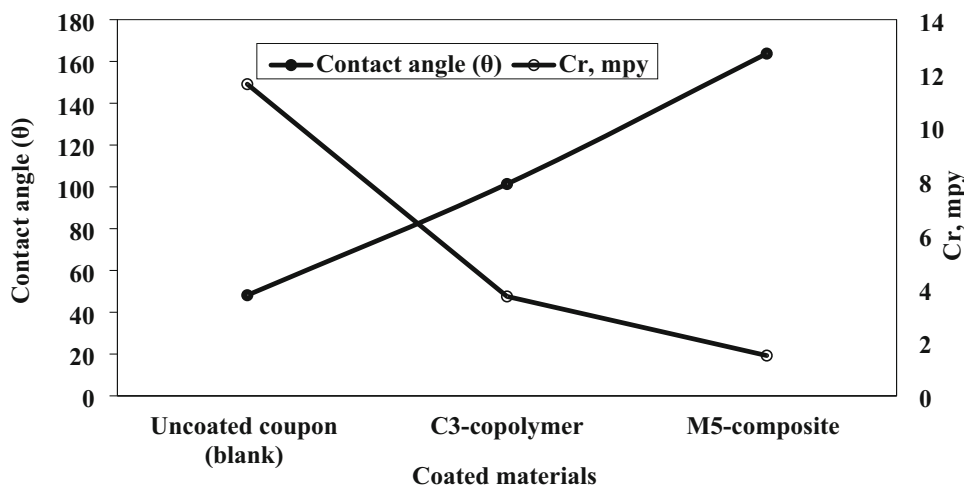


Fig. 8: Effect of the hydrophobicity character of the coating materials on the resultant contact angle and the corrosion rate at 100 ppm of the coating solution of the C3-copolymer and M5-composite, immersion time of 24 days, and 298 K

Meaning, the coupon surface coated with M5-nanocomposite can roll off more water droplets over the coupon surface than C3-copolymer. Therefore, the tendency of a water droplet to be more slippery on the coated coupon increased. From the previous results, the coating material with the minimum corrosion rate of 1.5 mpy and the highest contact angle of 132.35° was M5-nanocomposite.

Morphological structure study

The surface morphology of the uncoated and coated coupons carbon steel surfaces with C3-copolymer and M5-nanocomposite was analyzed by optical (visual examination) and scanning electron microscopies (SEM) as discussed in the following sections.

VISUAL EXAMINATION: Visual inspection is a conventional method used to depict the corrosion damage to the coated surface after its exposure to

corrosive media (brine water) using the weight loss technique under simulated oilfield production conditions.³⁰ The deterioration of the coupon surfaces depends on the degree of cracking and the porosity of the coated film when exposed to the corrosive media.³¹ Figures 9a–9d depict the surface topography of coupons coated with C3-copolymer and M5-nanocomposite after exposure to brine water (corrosive media) at a temperature of 298 K and 24 days. Compared with the uncoated coupons in Fig. 9a, the visual inspection in Fig. 9b showed that a high corrosion rate on all portions of the uncoating coupons was observed when the uncoated coupons were exposed to the brine water. Also, high localized corrosion pits were observed. The result in Fig. 9c indicates that the surface topography of the coated coupons with C3-nanocomposite was more corroded than that coated with M5-nanocomposite (Fig. 9d). Decreasing the deterioration of the coupon surface coated by the M5-nanocomposite was due to the following effects: First, the strength of the film formed on the surface of the coupon and second, the

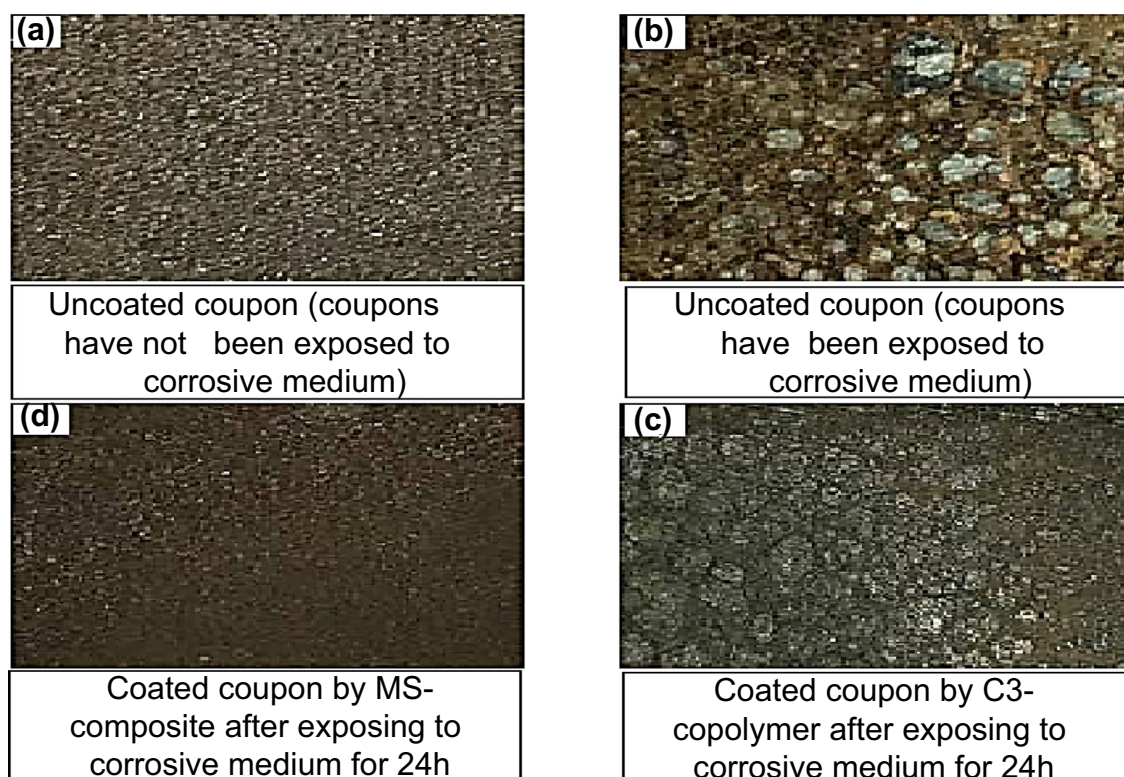


Fig. 9: (a–d): Microscopic examination of uncoated coupons (a) not immersed and (b) immersed in corrosive media (brine water) and immersed coupons coated with (c) C3-copolymer and (d) M5-composite at a concentration of 300 ppm of the coating solution, immersion time of 24 days in brine water solution, and 298 K [Coupons were photographed before and after completing the weight losses measurements]

roughness structure of the coated film. With the increase in the film roughness structure, the corrosion rate decreased.¹² However, improving the roughness degree resulted in the formation of heterogeneous-helical peak shape structures with varying heights on the coated surface. This helical shape caused the contact angle to increase, preventing the transfer of brine water to the underlying substrate, and consequently, the corrosion rate of the coupons coated by the M5-nanocomposite reduced to a minimum.

SCANNING ELECTRON MICROSCOPY (SEM) MEASUREMENTS: SEM technique was used to analyze the surface topography of the coupons coated with C3-copolymer and M5-nanocomposite after and before their exposure to the corrosive media, as illustrated in Figs. 10 a–10d. Figures 10 a–10d show the SEM images of uncoated and coated carbon steel coupons immersed in brine water solution containing 100 ppm concentration of C3-copolymer, and M5-nanocomposite solutions for 24 days. As shown in Fig. 10a, the surface of the uncoated coupon (blank)

showed a smooth and uniform surface without localized corrosion pits through the surface. As shown in Fig. 10b, the surface topography of the M5-nanocomposite showed a homogenous smooth surface without noticeable corrosion pits and/or pore holes on the coated coupon. The reason behind this was due to the surface topography of the coupons coated with M5-nanocomposite. The presence of E-silicate in the M5-nanocomposite increased the roughness and helical shape of the surface, causing the water droplet to slip off from the coupon surface; thereby, a smooth surface like the blank coupon was obtained.¹² From Fig. 10c, the surface topography of the C3-nanocomposite shows a significantly corroded area with small holes dipped on the surface. Furthermore, the surface of coated coupons with the C3-copolymer exhibited foldable dens and a highly wrinkled surface with internal and irregular cavities distributed through the C3-copolymer matrix. From the above findings, decreasing the corrosion rate of the coupon coated by C3-copolymer was due to the hydrophobic character and the folding structure of the C3-copolymer. The formation of few pores was attributed to the absence of E-silicate in the copolymer matrix.

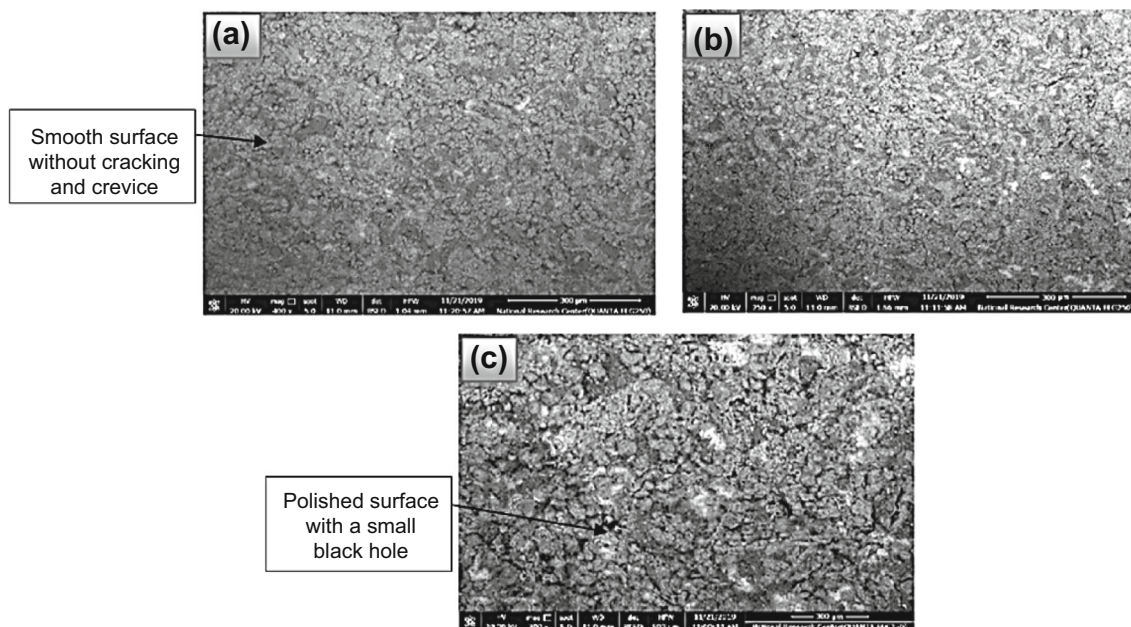


Fig. 10: (a–d) SEM images for (a) uncoated coupon, and coated coupon with (b) M5-nanocomposite and (c) C3-copolymer at a concentration of 100 ppm coating solution, immersion time of 24 days, and 298 K

Conclusions

Four hydrophobic and superhydrophobic coating materials were fabricated as new anticorrosive coating layers by incorporating the functionalized SiO₂-NPs into the C3-copolymer matrix. The corrosion inhibition efficiency of the coated materials was assessed using a rotating cage (RC) test. The surface topography of the coated surface with C3-copolymer and M5-nanocomposite after exposure to corrosive media was analyzed via optical microscopy and scanning electron microscopy (SEM). The results obtained revealed that the M5-nanocomposite possesses a higher corrosion inhibition efficiency of 99.63% and a contact angle of 161°. **Funding** Open access funding provided by The Science, Technology & Innovation Funding Authority (STDF) in cooperation with The Egyptian Knowledge Bank (EKB).

Conflict of interest The authors declare that there are no financial and personal relationships with other people or organizations that could inappropriately influence this work.

Open Access This article is licensed under a Creative Commons Attribution 4.0 International License, which permits use, sharing, adaptation, distribution and reproduction in any medium or format, as long as you give appropriate credit to the original author(s) and the source, provide a link to the Creative Commons licence, and indicate if changes were made. The images or other third party material in this article are included in the article's Creative

Commons licence, unless indicated otherwise in a credit line to the material. If material is not included in the article's Creative Commons licence and your intended use is not permitted by statutory regulation or exceeds the permitted use, you will need to obtain permission directly from the copyright holder. To view a copy of this licence, visit <http://creativecommons.org/licenses/by/4.0/>.

References

1. Noor El-Din, MR, Farag, RK, Elazbawy, OE, "Utilization of New Anionic Polymeric Surfactants for Corrosion Inhibition Enhancement in Petroleum Industries." *Int. J. Electrochem. Sci.*, **11** 815–835 (2016)
2. Farag, AA, Noor El-Din, MR, "The Adsorption and Corrosion Inhibition of Some Nonionic Surfactants on API X65 Steel Surface in Hydrochloric Acid." *Corr. Sci.*, **64** 174–183 (2012)
3. Amin, MA, Ahmed, MA, Arida, HA, Kandemirli, F, Saracoglu, M, Arslan, T, Basaran, MA, "Monitoring Corrosion and Corrosion Control of Iron in HCl by Non-Ionic Surfactants of the TRITON-X Series – Part II Temperature Effect, Activation Energies and Thermodynamics of Adsorption." *Corr. Sci.*, **53** (2) 540–548 (2011)
4. Tezdogan, T, Demirel, YK, "An Overview of Marine Corrosion Protection with a Focus on Cathodic Protection and Coatings." *Brodogradnja*, **62** (2) 49–59 (2014)
5. Rao, AV, Lathe, SS, Mahadik, SA, Kappenstein, C, "Mechanically Stable and Corrosion Resistant Superhydrophobic Sol-Gel Coatings on Copper Substrate." *Appl. Surf. Sci.*, **257** 5772–5776 (2011)

6. Wang, S, Jiang, L, “Definition of Superhydrophobic States.” *Adv. Eng. Mat.*, **19** (21) 3423–3424 (2007)
7. Maboudian, R, Ashurst, WR, Carraro, C, “Self-Assembled Monolayers as Anti-Stiction Coatings for MEMS: Characteristics and Recent Developments.” *Sens. Actuators*, **82** 219–223 (2000)
8. Grundmeier, G, Schmidt, W, Stratmann, M, “Corrosion Protection by Organic Coatings: Electrochemical Mechanism and Novel Methods of Investigation.” *Electrochimica Acta*, **45** 2515–2533 (2000)
9. Noor El-Din, MR, Mishrif, Marwa R, Morsi, RE, El-Sharaky, EA, Haseeb, ME, Ghanem, Rania TM, “A New Modified Low Energy Emulsification Method for Preparation of Water-in-Diesel Fuel Nanoemulsion as Alternative Fuel.” *J. Dispers. Sci. Technol.*, **38** (2) 248–255 (2017)
10. Wang, G, Wen, S, Qian, S, Wang, J, Wang, C, Chen, Y, “Synthesis of Novel Nano Hyperbranched Polymer Resin and its Corrosion Resistance in Coatings.” *Prog. Org. Coat.*, **140** 105496 (2020)
11. Zuev, VV, “The Mechanisms and Mechanics of the Toughening of Epoxy Polymers Modified with Fullerene C₆₀.” *Polym. Eng. Sci.*, **52** 2518–2522 (2012)
12. Noor-El-Din, MR, Hashem, AI, Morsi, RE, Abd El-Azeim, A, “New Superhydrophobic Nanocomposites as Anti-Corrosion Coating Films Part I Synthesis and Characterization of Poly(styrene/vinyl acetate) SiO₂ Nanocomposites as a Water-Repelling Surface via Nanoemulsion Polymerization Technique.” *J. Mol. Liq.*, **322** 114885 (2021)
13. Noor El-Din, MR, Hmeidan, Sabit MM, “New Modified Equations to Estimate the Percentage of Over Three Emulsifiers in Emulsifier Mixture to Form a Stable Emulsion.” *J. Surfactants Deterg.*, **24** 963–972 (2021)
14. Xiaoyu, H, Zhaohua, H, Junlian, H, “Copolymerization of Styrene and Vinyl Acetate by Successive Photoinduced Charge-Transfer Polymerization.” *J. Polym. Sci. A Polym. Chem.*, **38** 914–920 (2000)
15. Ye, L, Zhang, Y, Song, C, Li, Y, Jiang, B, “A Simple Sol-Gel Method to Prepare Superhydrophilic Silica Coatings.” *Mater. Lett.*, **188** 316–318 (2017)
16. Adnan, M, Lee, JK, “Highly Efficient Planar Heterojunction Perovskite Solar Cells with Sequentially Dip-Coated Deposited Perovskite Layers from a Non-Halide Aqueous Lead Precursor.” *RSC Adv.*, **10** 5454–5461 (2020)
17. Papavinasam, S, Revie, RW, Attard, MH, Demoz, A, Michaelian, K, “Comparison of Laboratory Methodologies to Evaluate Corrosion Inhibitors for Oil and Gas Pipelines.” *Corrosion*, **59** (10) 897–912 (2003)
18. Mishrif, Marwa R, Noor El-Din, MR, Khamis, EA, “Utilization of Ethoxylated Pentamine Oleamide as New Gemini Surfactants for Corrosion Inhibition Effectiveness in 1 M HCl Solution.” *Egypt. J. Pet.*, **27** 1357–1370 (2018)
19. JunFei, F, YiMin, X, Qiang, L, “Preparation of Polystyrene Spheres in Different Particle Sizes and Assembly of the PS Colloidal Crystals.” *Sci. China Tech. Sci.*, **53** (11) 3088–3093 (2010)
20. Wahab, MA, Kim, I, Ha, CS, “Microstructure and Properties of Polyimide/Poly (Vinylsilsesquioxane) Hybrid Composite Films.” *Polymer*, **44** (16) 4705–4713 (2003)
21. Klapiszewski, A, Bula, K, Sobczak, M, Jesionowski, T, “Influence of Processing Conditions on the Thermal Stability and Mechanical Properties of PP/Silica-Lignin Composites.” *Int. J. Polym. Sci.*, **2016** 1–9 (2016)
22. She, Z, Li, Q, Wang, Z, Tan, C, Zhou, J, Li, L, “Highly Anticorrosion, Self-Cleaning Superhydrophobic Ni–Co Surface Fabricated on AZ91D Magnesium Alloy.” *Surf. Coat. Tech.*, **251** 7–14 (2014)
23. Bogush, GH, Zukoski, CF, “Studies of the Kinetics of the Precipitation of Uniform Silica Particles Through the Hydrolysis and Condensation of Silicon Alkoxides.” *J. Colloid Interface Sci.*, **142** 1–18 (1991)
24. Cano, L, Di Mauro, AE, Striccoli, M, Curri, ML, Tercjak, A, “Optical and Conductive Properties of as-Synthesized Organic-Capped TiO₂ Nanorods Highly Dispersible in Polystyrene-Block-Poly (methyl methacrylate) Diblock Copolymer.” *ACS Appl. Mater. Interfaces*, **6** 11805 (2014)
25. Doncom, KEB, Blackman, LD, Wright, DB, Gibson, MI, O’Reilly, RK, “Dispersity Effects in Polymer Self-Assemblies: A Matter of Hierarchical Control.” *Chem. Soc. Rev.*, **46** 4119–4134 (2017)
26. Funke, W, “How Organic Coating Systems Protect Against Corrosion.” In: *Polymeric Materials for Corrosion Control*, pp. 222–228. American Chemical Society, US (1986)
27. Schmidt, DP, Shaw, BA, Sikora, E, Shaw, WW, “Corrosion Protection Assessment of Barrier Properties of Several Zinc-Containing Coating Systems on Steel in Artificial Seawater.” *Corrosion*, **62** 323–339 (2006)
28. Nešić, S, “Key Issues Related to Modelling of Internal Corrosion of Oil and Gas Pipelines – A Review.” *Corr. Sci.*, **49** (12) 4308–4338 (2007)
29. Al-Saadie, Khulood Abid Saleh, Haider, A, Al-Mashhdani, Yousif, “Corrosion Protection Study for Caron Steel in Seawater by Coating with SiC and ZrO₂ Nanoparticl.” *Am. J. Chem.*, **5** (1) 28–39 (2015)
30. Wu, LK, Zhang, XF, Hu, JM, “Corrosion Protection of Mild Steel by One-Step Electrodeposition of Superhydrophobic Silica Film.” *Corr. Sci.*, **85** 482–487 (2014)
31. Delimi, A, Galopin, E, Coffinier, Y, Pisarek, M, Boukherroub, R, Talhi, B, Szunerits, S, “Investigation of the Corrosion Behavior of Carbon Steel Coated with Fluoropolymer Thin Films.” *Surf. Coat. Tech.*, **205** 4011–4017 (2011)

Publisher’s Note Springer Nature remains neutral with regard to jurisdictional claims in published maps and institutional affiliations.